Support Information

Fibroblast activation protein-α-adaptive micelle reprogram stroma fibrosis for promoted anti-cancer drug delivery

Chao Teng [a], Beiyuan Zhang [a], Zhongyue Yuan[a], Zheng Kuang[a], Zhuodong Chai[a], Lianjie Ren[a,b], Chao Qin [a], Lei Yang[a], Xiaopeng Han [a*] and Lifang Yin[a*]

[a] School of Pharmacy, China Pharmaceutical University, Nanjing, 210009, PR China

[b] Center for Drug Evaluation, CFDA, Beijing,100022, PR China

Corresponding Author

Tel.: +86 2583271018; fax: +86 2583271018. E-mail address: nkhxp15@163.com (Xiaopeng Han)

Tel.: +86 2583271018; fax: +86 2583271018. E-mail address: lifangyin_@163.com (Lifang Yin)

Supplementary Figure Captions

Scheme S1. Synthesis of the FAP-α-sensitive pegylated Hyaluronic acid-Curcumin conjugate (PFHC).

Scheme S2. Synthesis of the non-FAP-α-sensitive pegylated Hyaluronic acid-Curcumin conjugate (PHC)(Ph= p-hydroxy-phenylalanine).

Figure S1. ^{1}H NMR spectrum of Z-Ala-pro-gly(Z-ARG) in DMSO-d6.

Figure S2. ^{1}H NMR spectrum of Ala-phe-gly(Z-AHG) in DMSO-*d*6.

Figure S3. Cleavage of Z-Ala-pro-gly after incubating with FAPα for 4 h. (A) 0h；(B) 4h.

Figure S4. Cleavage of Z-Ala-phe-gly after incubating with FAPα for 4 h. (A) 0h；(B) 4h.

Figure S5. ^{1}H NMR spectrum of PFHC in D_2O.

Figure S6. ^{1}H NMR spectrum of PFHC in D_2O after incubating with FAPα for 4 h.

Figure S7. ^{1}H NMR spectrum of PHC in D_2O after incubating with FAPα for 4 h.

Figure S8. *In vitro* DOX release profiles of DOX/PFHC and DOX/PHC NPs in different conditions. Data are presented as mean ± SD (n = 3).

Figure S9. The stability of nanapartilces formulations in 10 % plasma (A) and DMEM with 10% FBS(B) (Data are presented as mean ± SD (n = 3)).

Figure S10. The relative expressing levels of α-SMA in different cell lines with CLSM (bar=20 μm).

Figure S11. The relative expressing levels of FAP-α in in different cell lines with flow cytometry (a: control, b: NIH3T3 c: active NIH3T3).

Figure S12. The relative expressing levels of CD44 receptors in different cell lines. (A) Immunofluorescence staining analysis of CD44 receptors expression with CLSM (bar=100 μm). (B) Analysis of CD44 receptors expression with flow cytometry. (C) Analysis of CD44 receptors expression with WB.

Figure S13. Representative CLSM images of 4T1 cell lines following 2 h incubation with different formulations (DOX dosage: 5.0 μg/mL, bar=50 μm).

Figure S14. Representative CLSM images of active NIH3T3 cell lines following 2 h incubation with different formulations (DOX dosage: 5.0 μg/mL, bar=50 μm).

Figure S15. The cytotoxicity of Dox+Cur against different cell lines for 24h. (A)NIH3T3, (B) 4T1, (C) active NIH3T3 cells (mean ± SD, n = 3)(The concentration of free Cur was equal to that in DOX-loading nanoparticles with same DOX dosage).

Figure S16. (A-B)Ex vivo Dox fluorescence images of the major organs and tumor harvested from the 4T1-NIH3T3 bearing mice following different times intravenous injection of NPs (DOX:5mg/kg). (C)Quantitative analysis of relative organ and tumor accumulation at 8 h (*P≤0.05, indicates ± SD, n = 3).

Figure S17. Plasma concentration-time curves of DOX in rats after intravenous administration with different DOX formulations at a dose of 5 mg/kg DOX (n = 3, mean ± SD).

Figure S18. Expression of FAPα by western blot in 4T1 tumor tissues (30μg of rhFAPα used as control).

Figure S19. H&E staining of major organs after the last treatment (bar= 50 μm).

Figure S20. Morphological evaluations of tumor sites. (A) In situ cell death detection of tumor tissue (TUNEL);(B) *In vivo* evaluation of tumor proliferation level by Ki-67 immunohistochemistry (*P≤0.05, **P≤0.01, indicates ± SD, n = 3).

Figure S21. Semi-quantitative analysis of Masson staining and α-SMA by immunofluorescent staining (*P≤0.05, indicates ± SD, n = 3).

Figure S22. Micro-distribution of NPs in tumor mass after last treatment. (bar=20 μm)

Figure S23. Semi-quantitative analysis of TGF-beta and MCP-1 by immunofluorescent staining (*P≤0.05, indicates ± SD, n = 3).

Table S1. Characterizations of the micelles. (indicates ± SD, n = 3)

Table S2. Pharmacokinetic parameters of Dox and DOX-loading NPs in mice after a single intravenous administration at the dose of 5 mg/kg (*n* = 3).

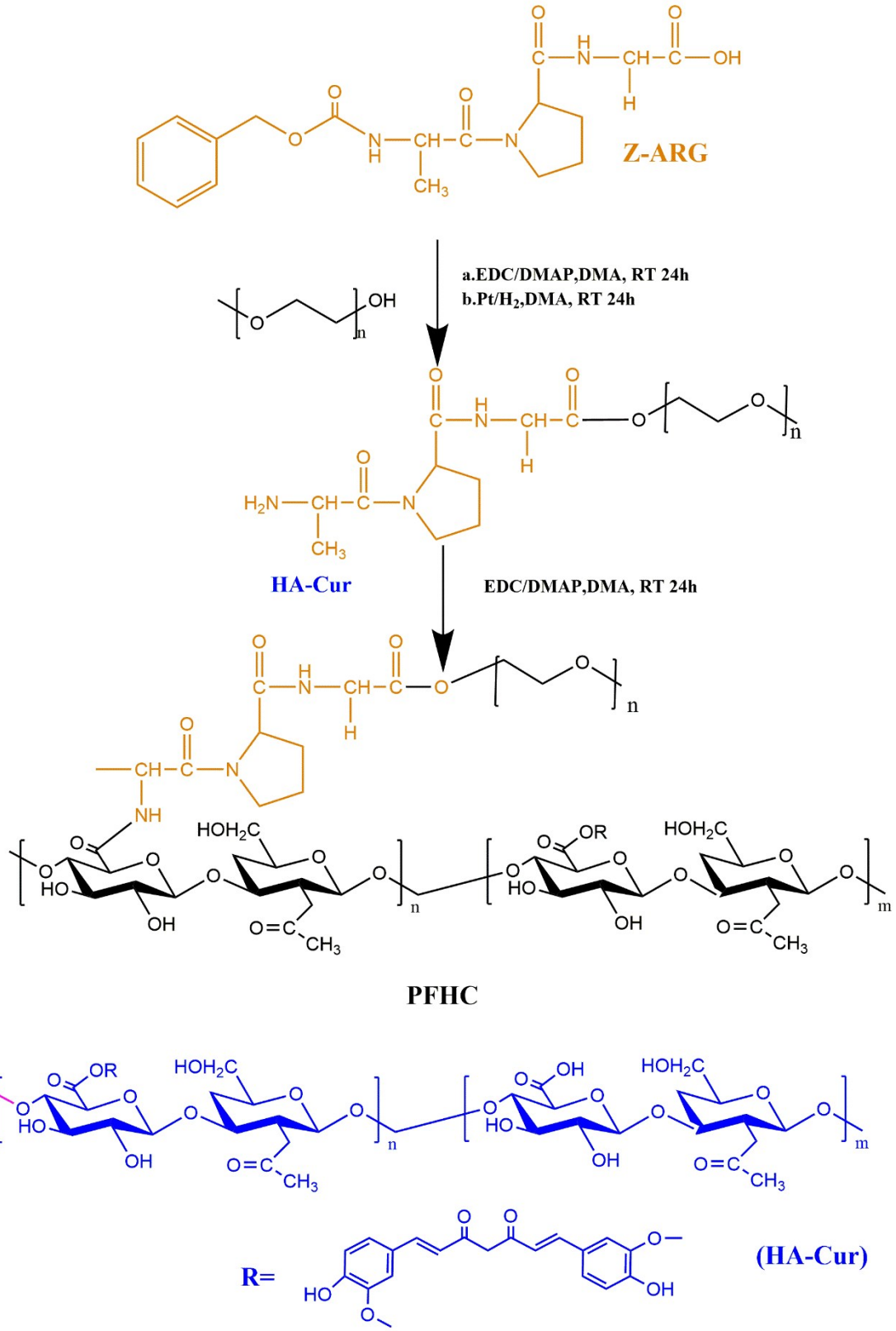

Scheme S1. Synthesis of the FAP-α-sensitive pegylated Hyaluronic acid-Curcumin conjugate (PFHC).

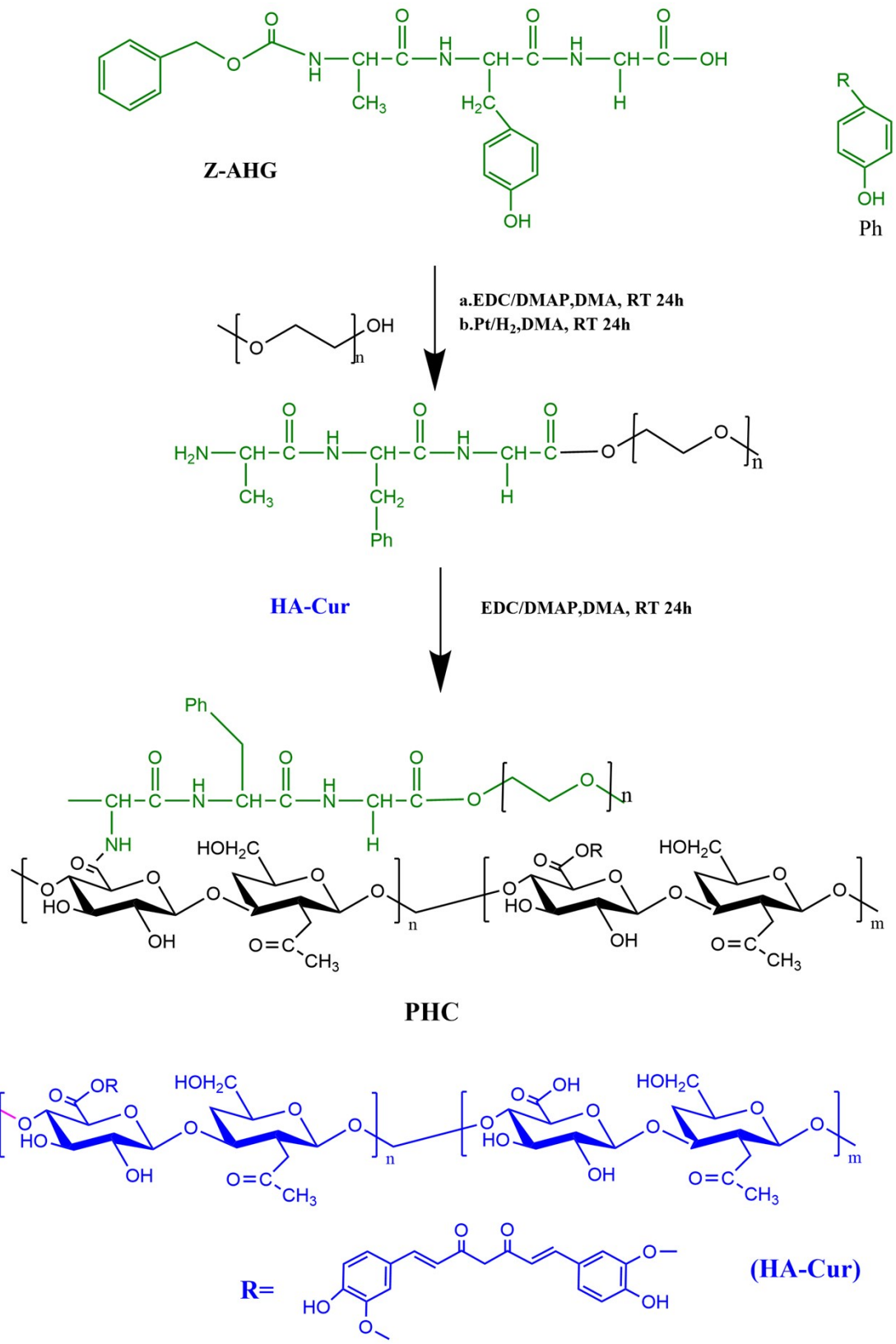

Scheme S2. Synthesis of the non-FAP-α-sensitive pegylated Hyaluronic acid-Curcumin conjugate (PHC)(Ph= p-hydroxy-phenylalanine).

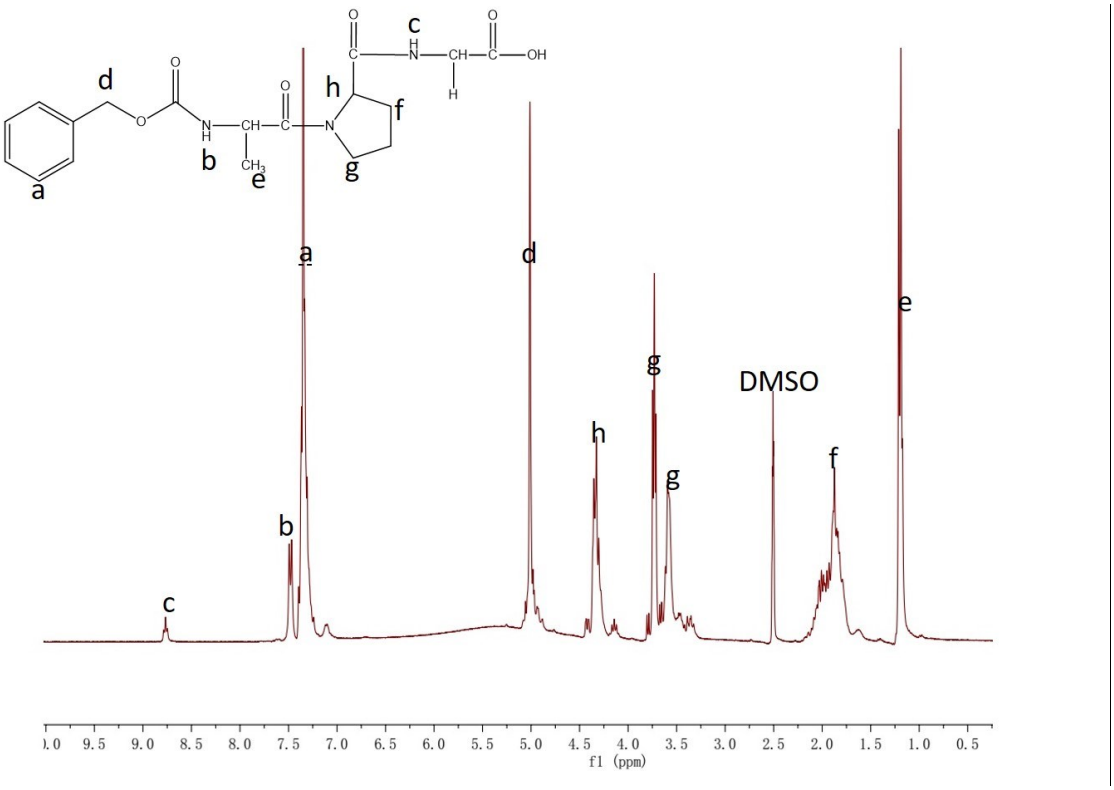

Figure S1. [1]H NMR spectrum of Z-Ala-pro-gly(Z-ARG) in DMSO-d6.

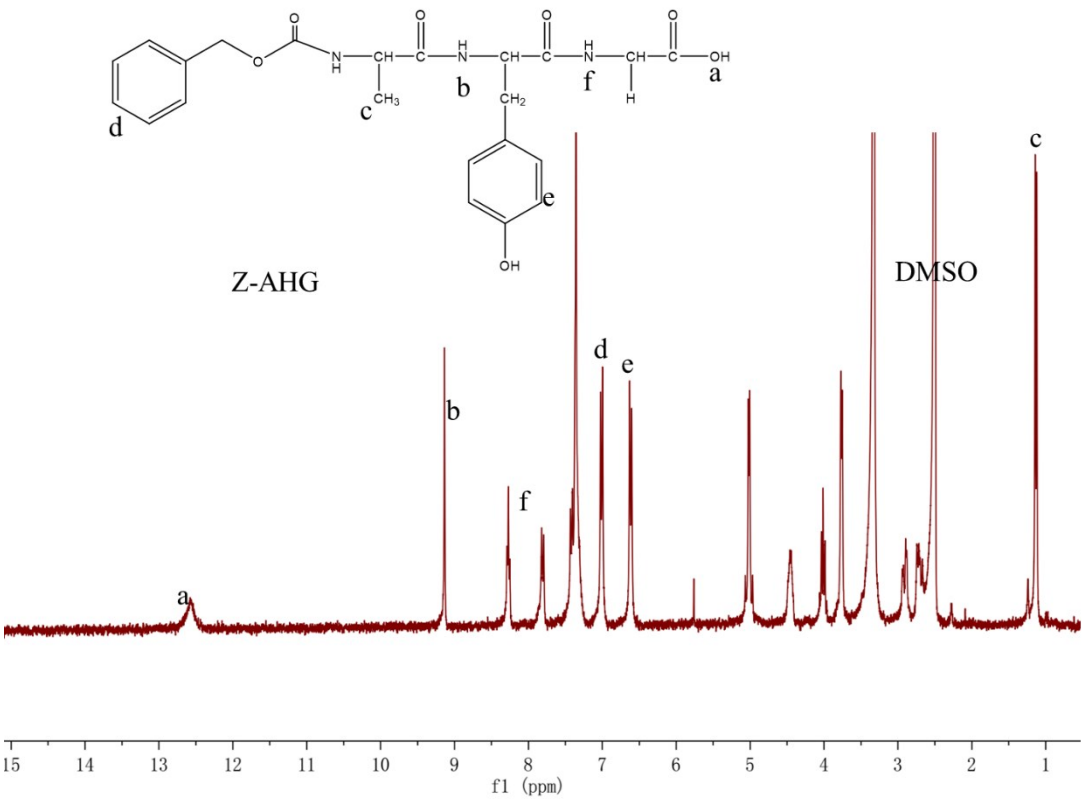

Figure S2. [1]H NMR spectrum of Ala-phe-gly(Z-AHG) in DMSO-*d*6.

Figure S3. Cleavage of Z-Ala-pro-gly after incubating with FAPα for 4 h. (A) 0h；(B)

4h.

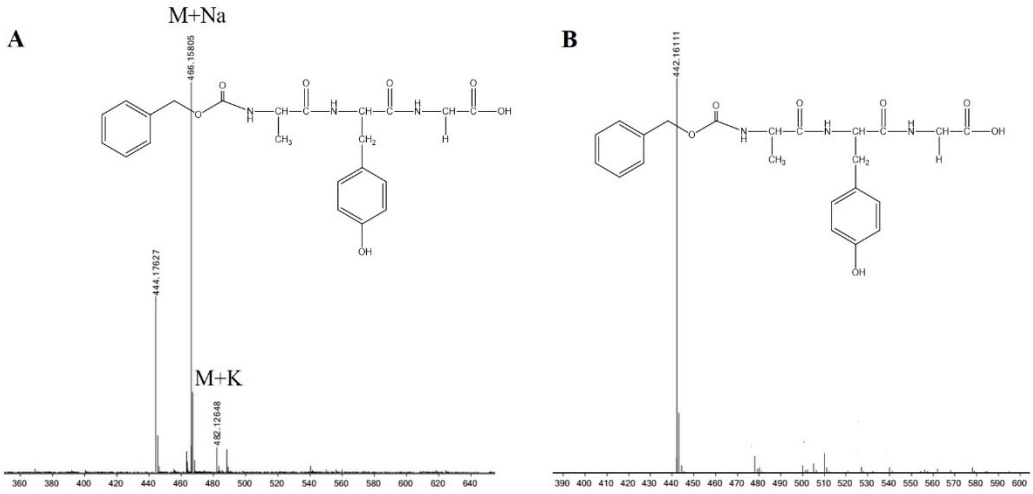

Figure S4. Cleavage of Z-Ala-phe-gly after incubating with FAPα for 4 h. (A) 0h；(B) 4h.

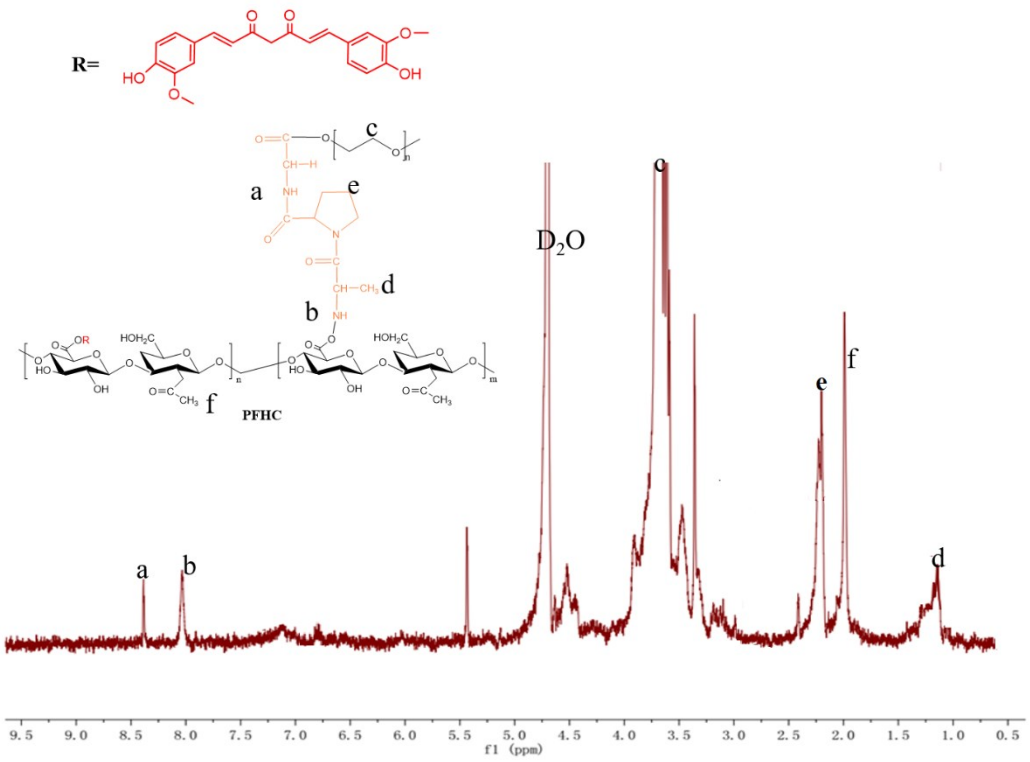

Figure S5. ^{1}H NMR spectrum of PFHC in D_2O.

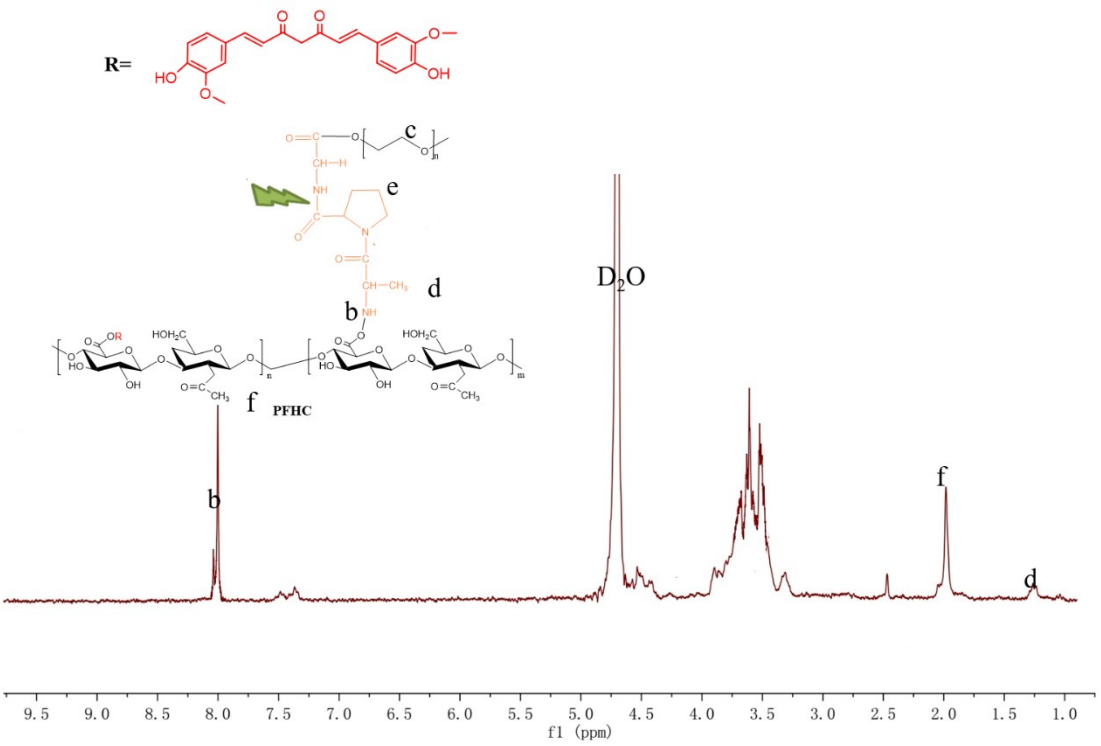

Figure S6. ^{1}H NMR spectrum of PFHC in D_2O after incubating with FAPα for 4 h.

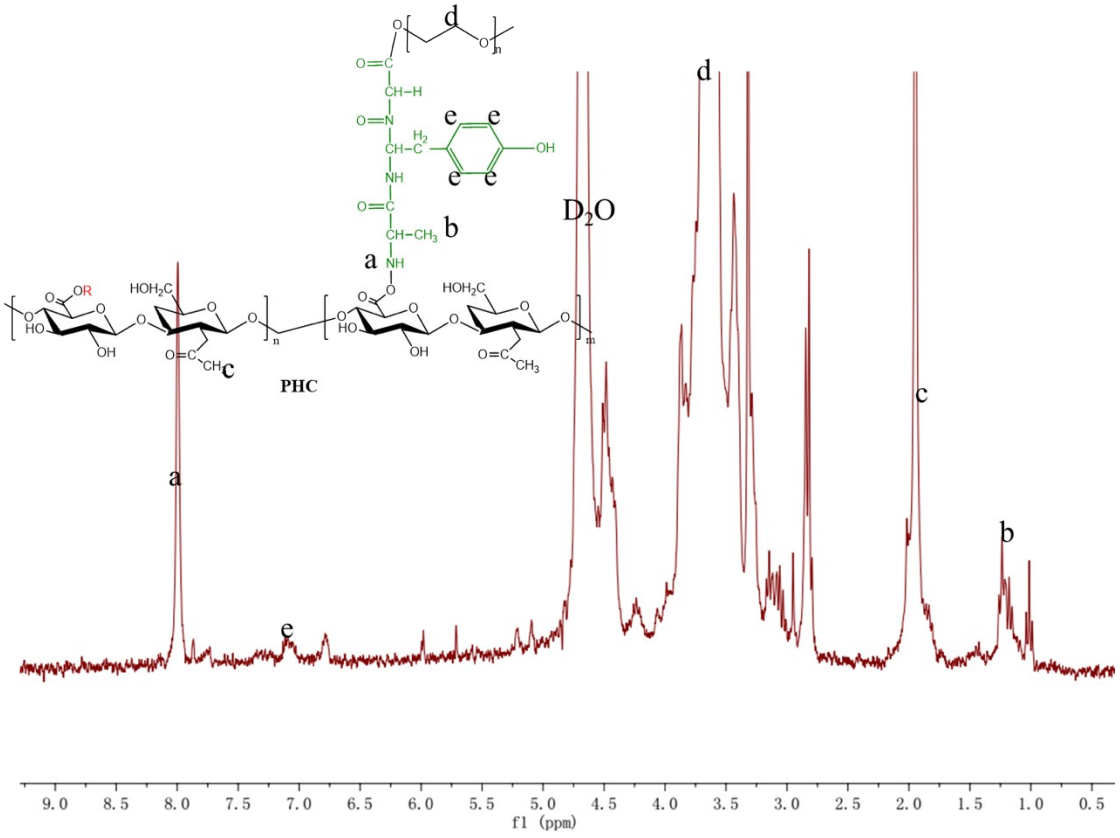

Figure S7. ^{1}H NMR spectrum of PHC in D_2O after incubating with FAPα for 4 h.

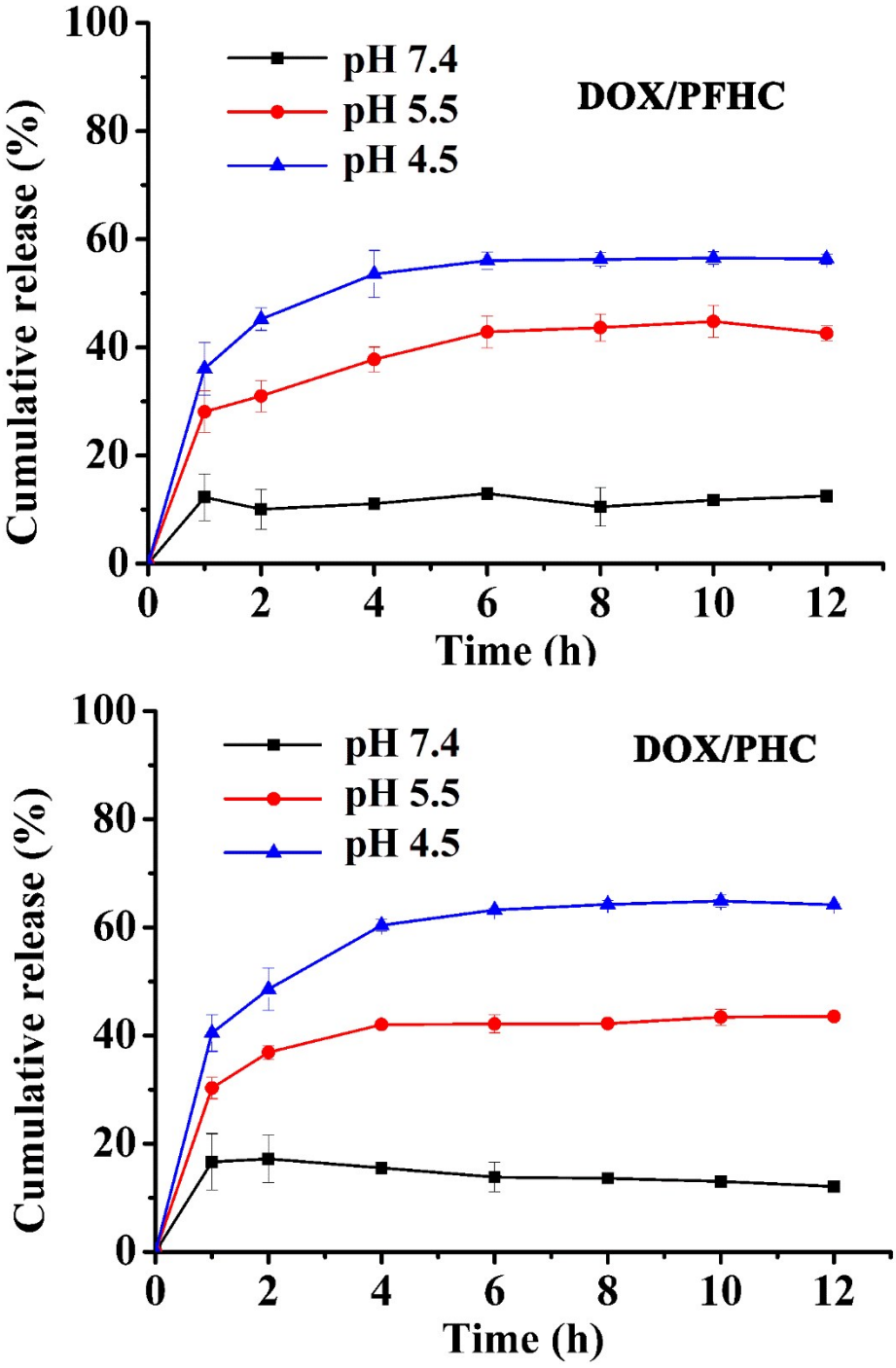

Figure S8. *In vitro* DOX release profiles of DOX/PFHC and DOX/PHC NPs in different conditions. Data are presented as mean ± SD (n = 3).

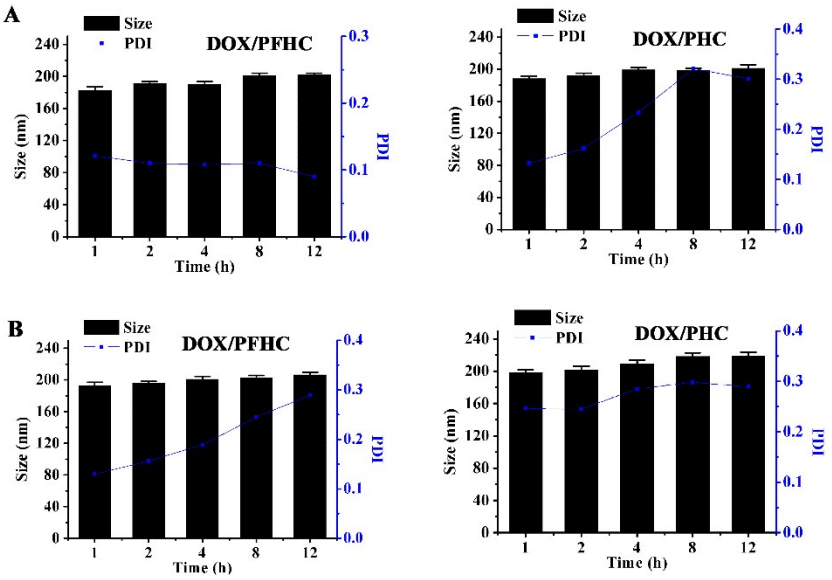

Figure S9. The stability of nanapartilces formulations in 10 % plasma (A) and DMEM with 10% FBS(B) (Data are presented as mean ± SD (n = 3)).

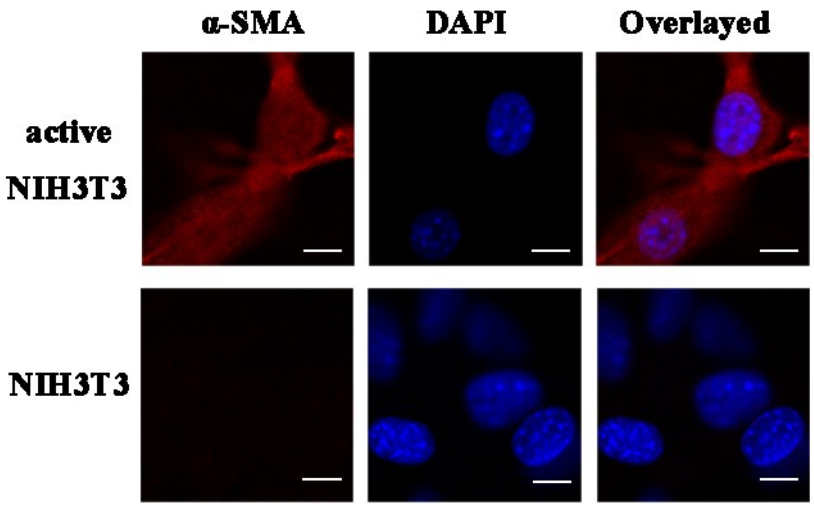

Figure S10. The relative expressing levels of α-SMA in different cell lines with CLSM (bar=20 μm).

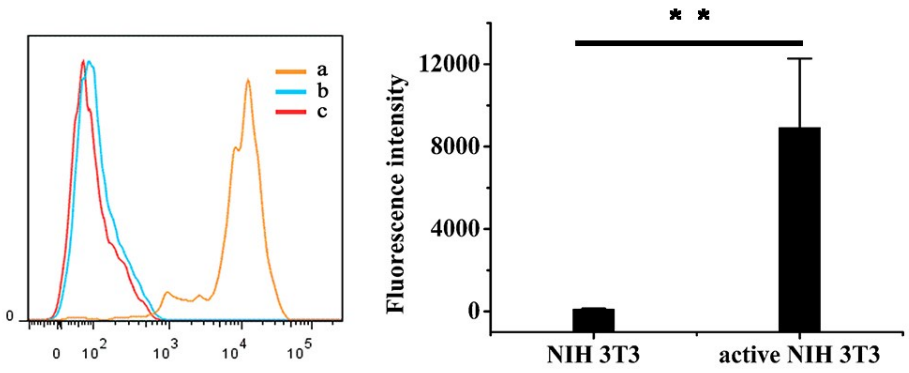

Figure S11. The relative expressing levels of FAP-α in in different cell lines with flow cytometry (a: active NIH3T3, b: NIH3T3 c: control).

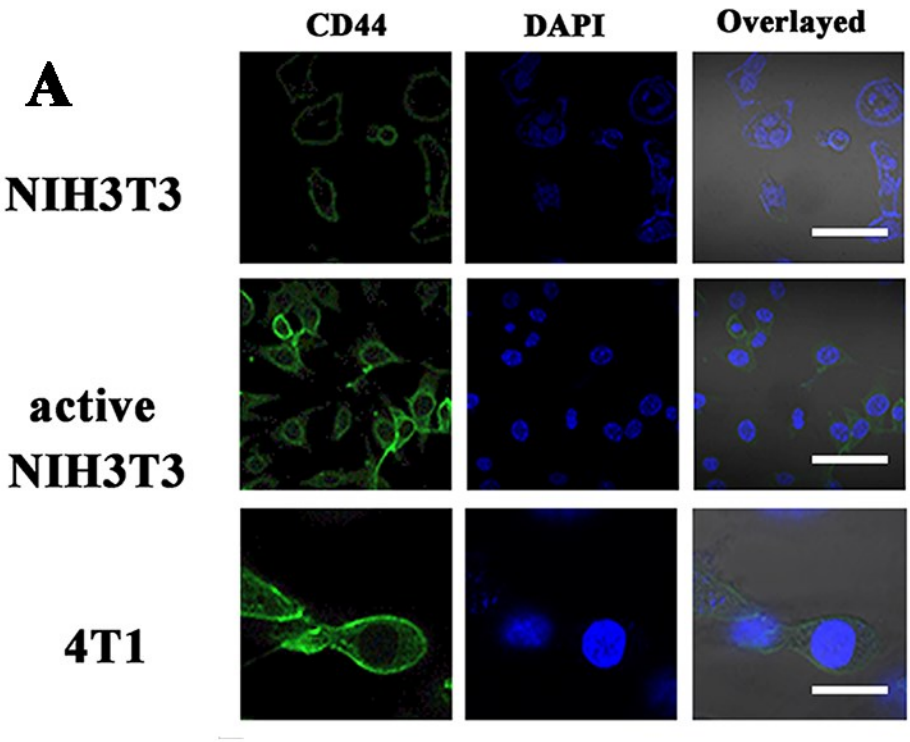
A
CD44
DAPI
Overlayed
NIH3T3
active NIH3T3
4T1

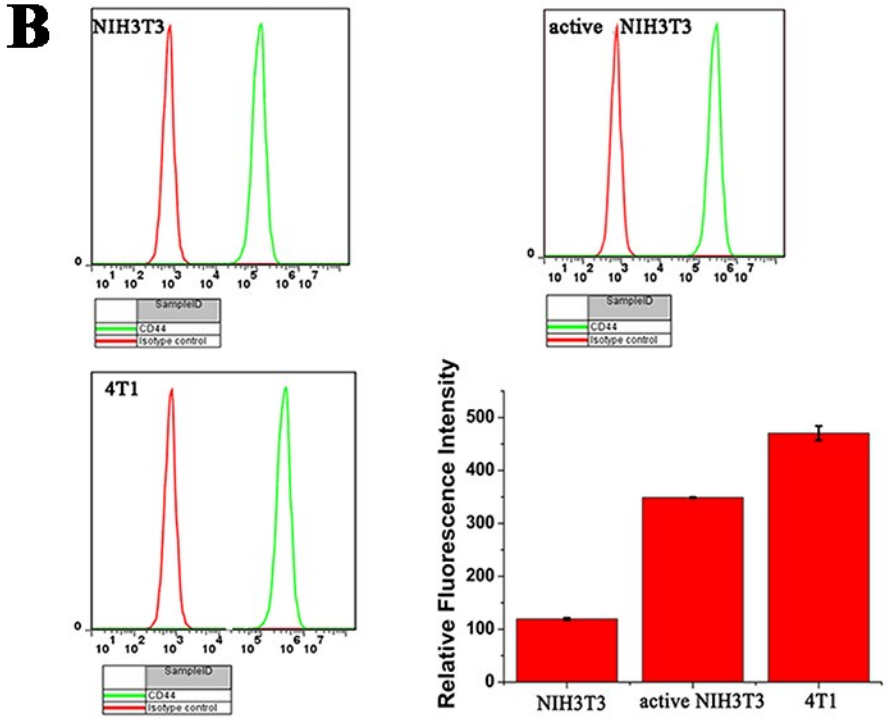
B
NIH3T3
active NIH3T3
4T1
SampleID
CD44
Isotype control
Relative Fluorescence Intensity
0
100
200
300
400
500
NIH3T3
active NIH3T3
4T1

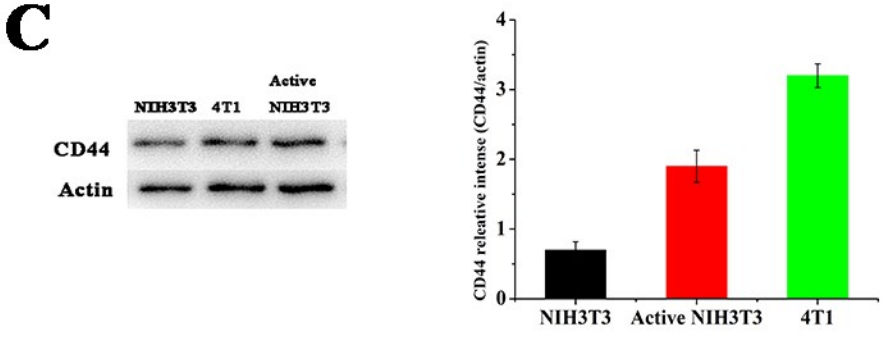
C
NIH3T3
4T1
Active NIH3T3
CD44
Actin
CD44 releative intense (CD44/actin)
0
1
2
3
4
NIH3T3
Active NIH3T3
4T1

Figure S12. The relative expressing levels of CD44 receptors in different cell lines. (A) Immunofluorescence staining analysis of CD44 receptors expression with CLSM (bar=100 μm). (B) Analysis of CD44 receptors expression with flow cytometry. (C) Analysis of CD44 receptors expression with WB.

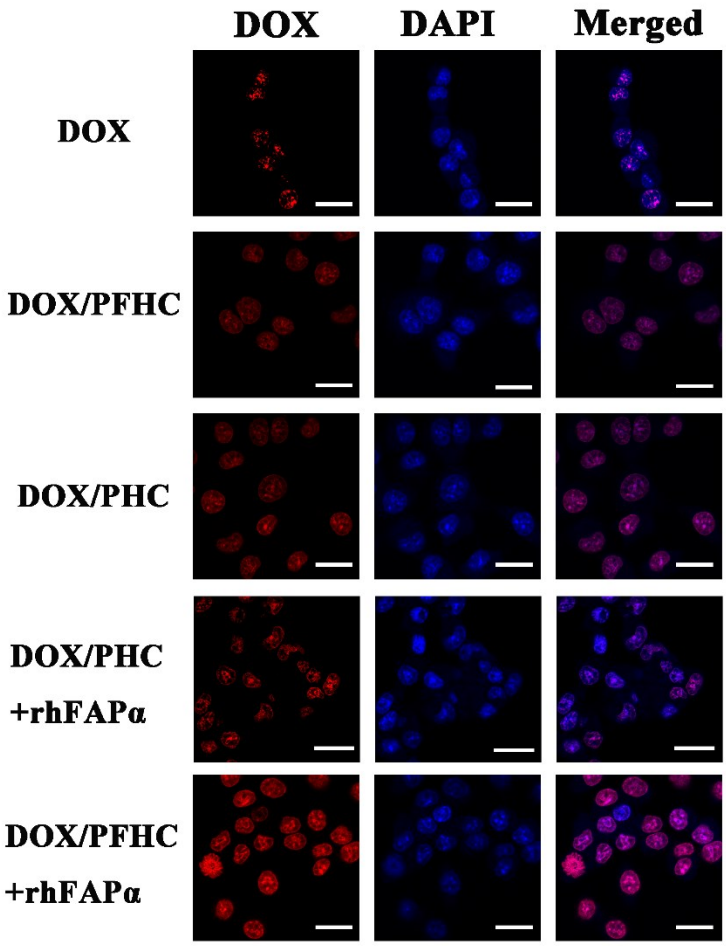

Figure S13. Representative CLSM images of 4T1 cell lines following 2 h incubation with different formulations (DOX dosage: 5.0 μg/mL, bar=50 μm).

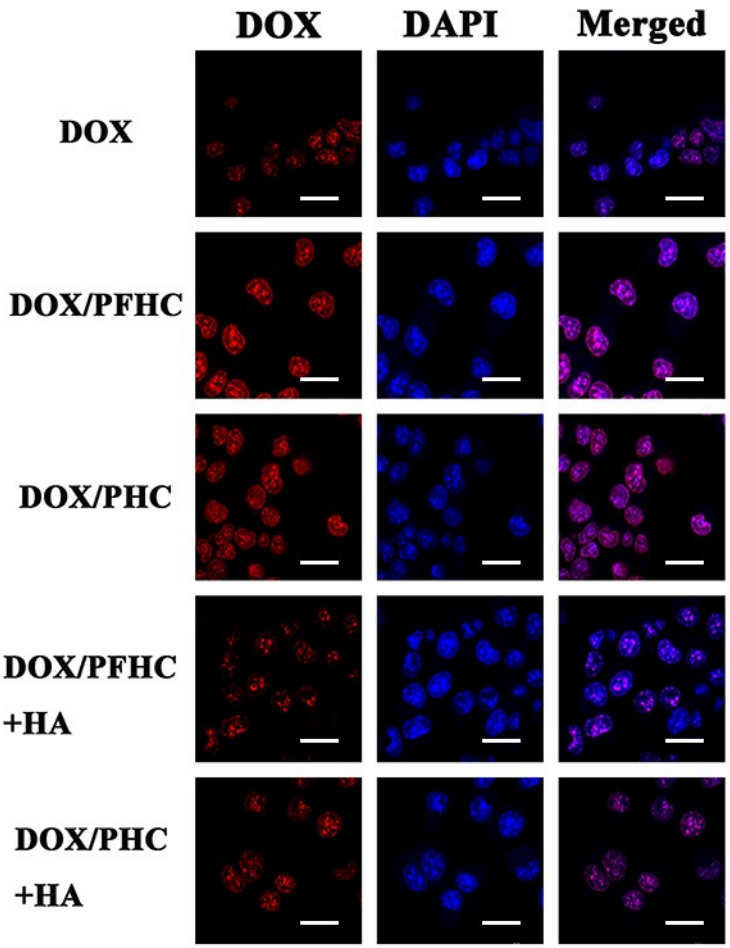

Figure S14. Representative CLSM images of active NIH3T3 cell lines following 2 h incubation with different formulations (DOX dosage: 5.0 μg/mL, bar=50 μm).

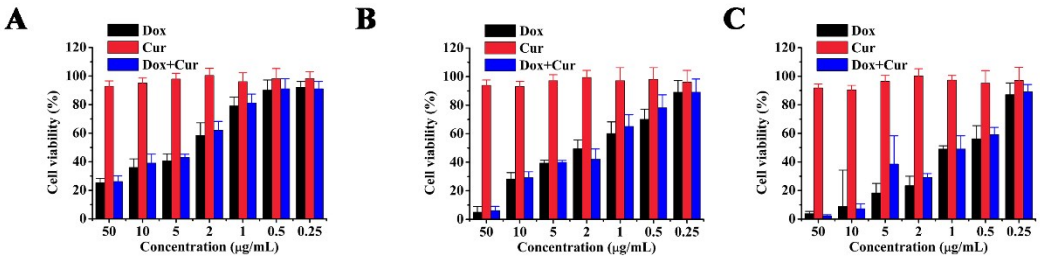

Figure S15. The cytotoxicity of Dox+Cur against different cell lines for 24h. (A)NIH3T3, (B) 4T1, (C) active NIH3T3 cells (mean ± SD, n = 3)(The concentration of free Cur was equal to that in DOX-loading nanoparticles with same DOX dosage).

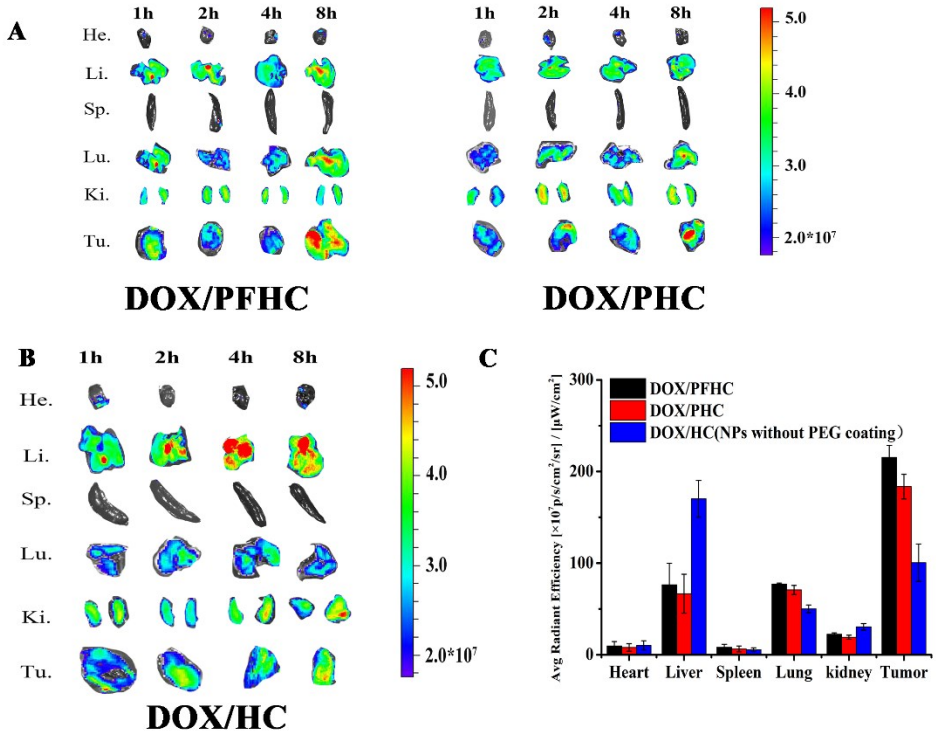

Figure S16. (A-B)Ex vivo Dox fluorescence images of the major organs and tumor harvested from the 4T1-NIH3T3 bearing mice following different times intravenous injection of NPs (DOX:5mg/kg). (C)Quantitative analysis of relative organ and tumor accumulation at 8 h (*P≤0.05, indicates ± SD, n = 3).

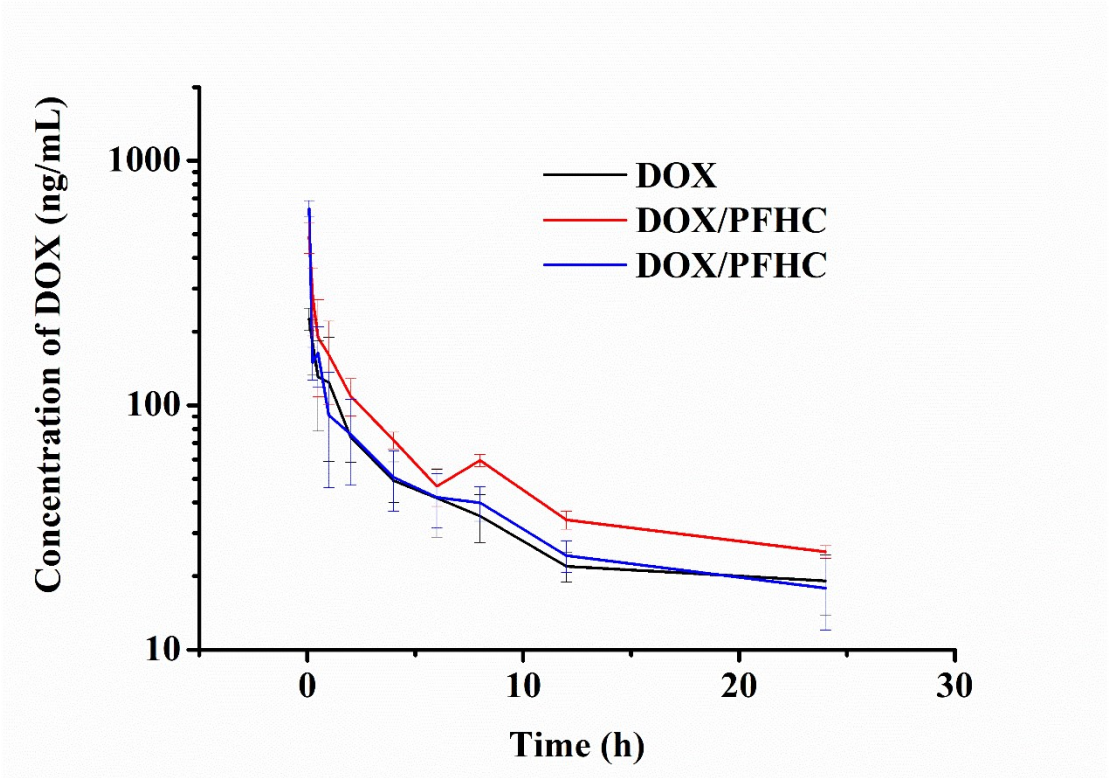

Figure S17. Plasma concentration-time curves of DOX in rats after intravenous administration with different DOX formulations at a dose of 5 mg/kg DOX (n = 3, mean ± SD) .

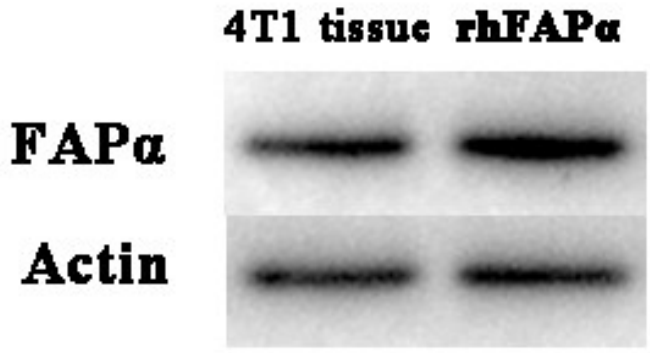

Figure S18. Expression of FAPα by western blot in 4T1 tumor tissues (30μg of rhFAPα used as control).

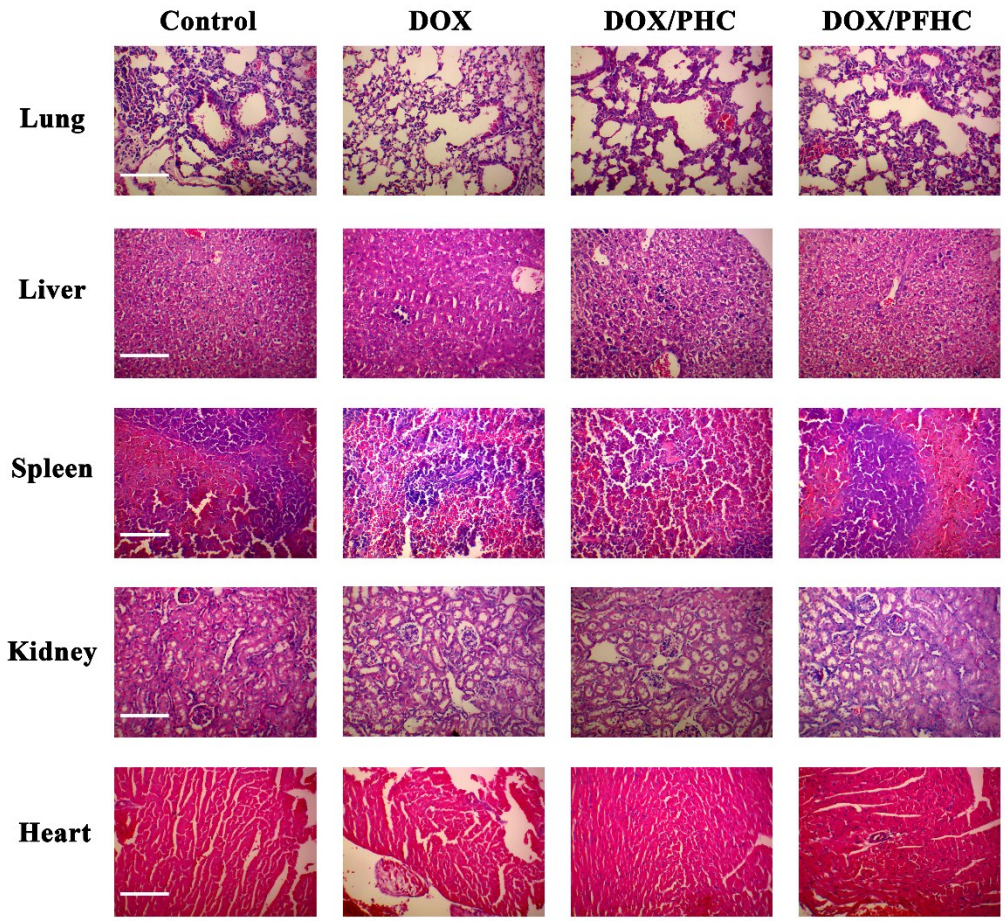

Figure S19. H&E staining of major organs after the last treatment (bar= 50 μm).

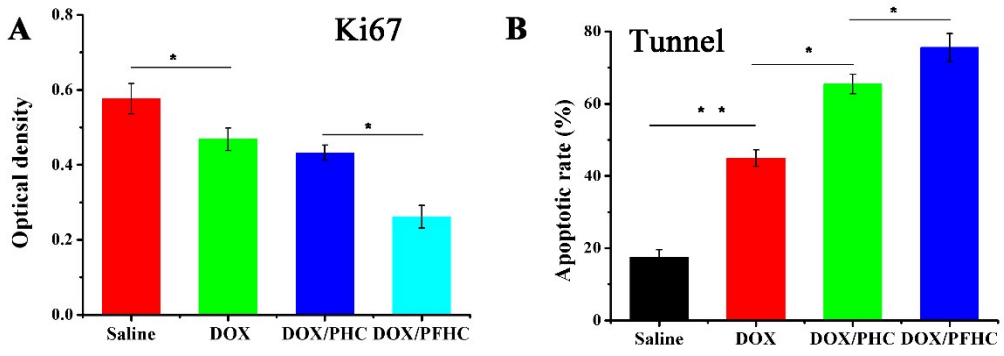

Figure S20. Morphological evaluations of tumor sites. (A) In situ cell death detection of tumor tissue (TUNEL);(B) *In vivo* evaluation of tumor proliferation level by Ki-67 immunohistochemistry (*P≤0.05, **P≤0.01, indicates ± SD, n = 3).

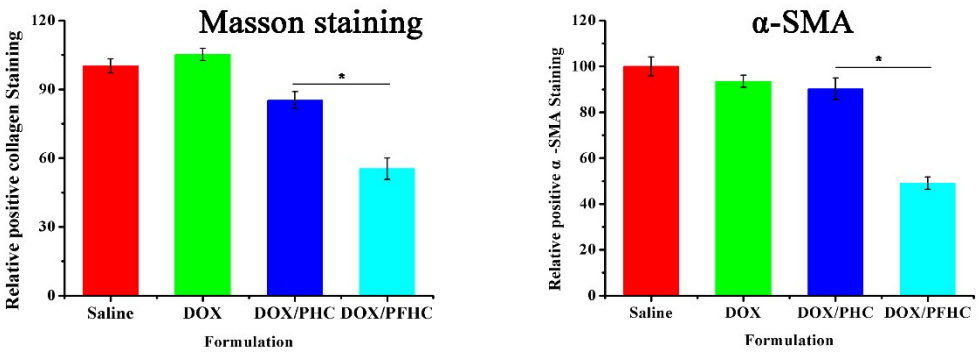

Figure S21. Semi-quantitative analysis of Masson staining and α-SMA by immunofluorescent staining (*P≤0.05, indicates ± SD, n = 3).

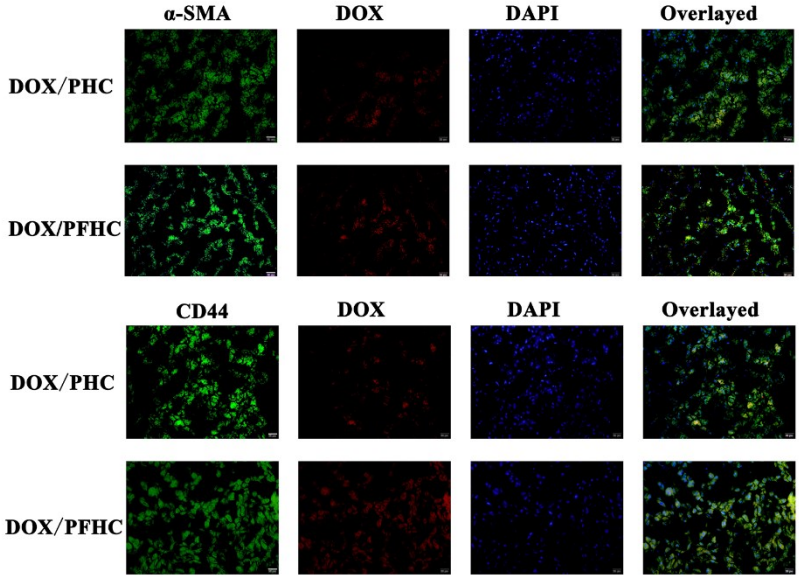

Figure S22. Micro-distribution of NPs in tumor mass after last treatment. (bar=20 μm)

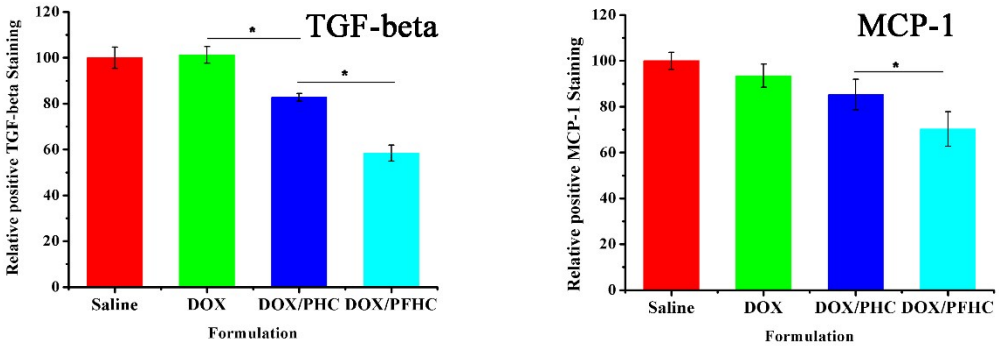

Figure S23. Semi-quantitative analysis of TGF-beta and MCP-1 by immunofluorescent staining (*P≤0.05, indicates ± SD, n = 3).

Table S1. Characterizations of the micelles. (indicates ± SD, n = 3)

Name	Size(nm)	PDI	Zeta potential (mv)	DL (%)	EE (%)
DOX/PHC	178.1±2.5	0.202±0.08	0	9.8±0.15	98±0.23
DOX/PFHC	167.3±1.3	0.12±0.02	-3.2±0.3	9.9±0.13	95±0.21

Table S2. Pharmacokinetic parameters of Dox and DOX-loading NPs in mice after a single intravenous administration at the dose of 5 mg/kg (n = 3).

Parameter	Units	DOX	DOX/PHC	DOX/PFHC
$AUC_{(0-t)}$	μg/L*h	1118.44±103.51	1184.44±367.65	1358.33±132.92
$t_{1/2}$	h	4.47±1.13	13.6±4.01	13.92±1.9